Journal of Hazardous Materials 192 (2011) 1114–1121

Contents lists available at ScienceDirect

Journal of Hazardous Materials

journal homepage: www.elsevier.com/locate/jhazmat

Novel hollow microspheres of hierarchical zinc–aluminum layered double hydroxides and their enhanced adsorption capacity for phosphate in water

Jiabin Zhou[a,b], Siliang Yang[b], Jiaguo Yu[a,*], Zhan Shu[a]

[a] State Key Laboratory of Advanced Technology for Materials Synthesis and Processing, Wuhan University of Technology, 122 Luoshi Road, Wuhan 430070, PR China
[b] School of Resources and Environmental Engineering, Wuhan University of Technology, 122 Luoshi Road, Wuhan 430070, PR China

ARTICLE INFO

Article history:
Received 9 February 2011
Received in revised form 29 May 2011
Accepted 7 June 2011
Available online 12 June 2011

Keywords:
Zn–Al LDHs
Hierarchical porous structures
Hollow microspheres
Phosphate
Adsorption isotherm
Kinetics

ABSTRACT

Hollow microspheres of hierarchical Zn–Al layered double hydroxides (LDHs) were synthesized by a simple hydrothermal method using urea as precipitating agent. The morphology and microstructure of the as-prepared samples were characterized by X-ray diffraction (XRD), field-emission scanning electron microscopy (FE-SEM), nitrogen adsorption–desorption isotherms and fourier transform infrared (FTIR) spectroscopy. It was found that the morphology of hierarchical Zn–Al LDHs can be tuned from irregular platelets to hollow microspheres by simply varying concentrations of urea. The effects of initial phosphate concentration and contact time on phosphate adsorption using various Zn–Al LDHs and their calcined products (LDOs) were investigated from batch tests. Our results indicate that the equilibrium adsorption data were best fitted by Langmuir isothermal model, with the maximum adsorption capacity of 54.1–232 mg/g; adsorption kinetics follows the pseudo-second-order kinetic equation and intra-particle diffusion model. In addition, Zn–Al LDOs are shown to be effective adsorbents for removing phosphate from aqueous solutions due to their hierarchical porous structures and high specific surface areas.

1. Introduction

Eutrophication is a natural process, in which untreated sewage effluents and agricultural run-off-based fertilizers were recognized as the main sources for eutrophication of rivers, lakes, and seas [1]. Anthropogenic activities have significantly accelerated the rate at which nutrients enter ecosystems in the past decades. Nowadays eutrophication has become a widespread polluting source that should be under control for both point and nonpoint sources of pollution. Moreover, phosphorus is often regarded as the main culprit in cases of eutrophication in lakes subjected to point source pollution from sewage discharge [2].

Wastewater from industrial discharge, agricultural runoff, and household activities involves considerable amounts of soluble phosphate which offers excessive nutrients in natural waters and thus promotes eutrophication. Phosphate removal from wastewater has been extensively studied over the past decades. To date, the main commercial processes for removing phosphorus from wastewater effluents are chemical precipitation with iron [3,4], alum [5,6], or lime [7,8], but the sludge handling makes it difficult to recycle precipitates in a cost-effective way. Biological removal of phosphate from wastewater has been developed since 1950s, but only 10–30% of phosphate can be removed [9]. On the other hand, adsorption is one of the most effective and economical technologies. Developing low-cost adsorbents in wastewater treatment has been investigated in recent years. Examples are red mud [10], fly ash [11], blast furnace slag [12,13], alum sludge [14,15], aluminum- and iron-rich residues [16], iron hydroxide–eggshell waste [17] and calcite [18]. In general, novel materials with high surface area, large pore volume and selective adsorption sites are crucial for effective utilization as adsorbents [19,20]. Recently, hierarchical materials with interconnected pore structures on micro-meso-macro length scales have received great attention in that they combine high surface area micro- and meso-porosity with accessible diffusion pathways of macroporous networks and thus exhibit excellent adsorption capacity for removing contaminants [21,22]. In our previous work, the controlled synthesis of hierarchically nanoporous materials such as Al_2O_3 [23–26], TiO_2 [27,28], WO_3 [29,30], $Ni(OH)_2$, NiO [31] and MgO [32] with high adsorption and catalytic efficiency has been successfully achieved.

Layered double hydroxides (LDHs), known as anionic clays, and their calcined products have been widely studied as catalysts, drug delivery materials, adsorbents, polymer additives and flame retardants. The general formula of LDHs can be expressed as $[M_{1-x}^{2+}M_x^{3+}(OH)_2]\,[A^{n-}]_{x/n}\cdot yH_2O$, where M^{2+} and M^{3+} are di- and trivalent metal cations in the octahedral positions of brucite-like layers yielding excessive positive charge and A^{n-} is the interlayer counter anions which balance the positive charges on the layers.

* Corresponding author at: State Key Laboratory of Advanced Technology for Materials Synthesis and Processing, Wuhan University of Technology, 122 Luoshi Road, Wuhan 430070, Hubei, PR China. Tel.: +86 27 87871029; fax: +86 27 87879468.
E-mail address: jiaguoyu@yahoo.com (J. Yu).

0304-3894/$ – see front matter © 2011 Elsevier B.V. All rights reserved.
doi:10.1016/j.jhazmat.2011.06.013

Table 1
Effects of the concentration of urea and calcination temperatures on textural properties of the Zn–Al LDHs and LDOs samples.

Samples	Urea (M)	Temperature (°C)	S_{BET} (m^2/g)	Pore volume (cm^3/g)	Average pore size (nm)
LDH (0.1)	0.1	–	37.1	0.08	9.1
LDH (0.4)	0.4	–	64.9	0.19	11.7
LDO (0.1)	0.1	300	136.6	0.24	7.0
LDO (0.4)	0.4	300	158.3	0.29	7.4

With relatively large surface areas and high anion-exchange capacity, LDHs have been previously employed in several studies for removing phosphate from simple electrolytes [33–35], drain effluents [36] and seawaters [37].

Nevertheless, it is still a great challenge to develop facile, environmentally friendly and versatile methods for the synthesis of layered double hydroxides with tunable morphology, textures, chemical compositions and desirable functions. Furthermore, in-depth understanding of underlying adsorption mechanisms of phosphate on LDHs is critical for their practical utilization as adsorbents in wastewater treatment. This study is the first report on the morphology evolution and formation mechanisms of hierarchical Zn–Al LDHs as well as their adsorption performance for phosphate in water. Our results gain new insights into morphology control and enhancement of adsorption capacity of hierarchically porous LDHs materials.

2. Experimental

2.1. Materials

All the reagents were of analytical grade and were used without further purification. The stocking solutions of 500 mg/L phosphate were initially prepared by dissolving a certain amount of KH_2PO_4 powders in distilled water. Artificial phosphate solutions were used throughout the adsorption tests.

2.2. Preparation of LDHs

Zn–Al LDHs were synthesized by a hydrothermal method using urea as precipitating agent. In a typical synthesis process, $Zn(NO_3)_2{\cdot}6H_2O$ (3.75 g) and $Al(NO_3)_3{\cdot}9H_2O$ (1.49 g) were dissolved in 100 mL of distilled water. The concentration of urea was varied from 0.1 M to 0.4 M. The mixed solutions were stirred for 1 h at room temperature. Then the homogeneous solution were transferred into a Teflon-lined autoclave and heated at 150 °C for 36 h. After cooling to room temperature, the solid precipitate was collected by centrifugation and washed three times with water and ethanol, respectively. The washed samples were dried in an oven at 80 °C for 4 h to obtain Zn–Al LDHs products. Finally, a part of the LDHs products were calcined at 300 °C for 6 h, which were denoted as Zn–Al LDOs. Table 1 shows the detailed experimental conditions for the preparation of the samples.

2.3. Characterization methods

X-ray diffraction (XRD) patterns were obtained on an X-ray diffractometer (type HZG41B-PC) using Cu Kα radiation at a scan rate of 0.05° $2\theta\,s^{-1}$ to determine the phase structures of the obtained samples. The accelerating voltage and applied current were 40 kV and 80 mA, respectively. The morphologies of all samples were observed by an S-4800 Field Emission Scanning electron microscopy (FESEM, Hitachi, Japan) at an accelerating voltage of 10 kV and linked with an Oxford Instruments X-ray analysis system. The Brunauer–Emmett–Teller (BET) surface area of the powders was analyzed by nitrogen adsorption in a Micromeritics ASAP 2020 nitrogen adsorption apparatus (U.S.). All the samples were degassed at 150 °C prior to the nitrogen-adsorption measurements. The BET surface area was determined by a multipoint BET method using the adsorption data in the relative pressure (P/P_0) range of 0.05–0.3. A desorption isotherm was used to determine the pore-size distribution by the Barret–Joyner–Halender (BJH) method. The nitrogen-adsorption volume at the relative pressure (P/P_0) of 0.994 was used to determine the pore volume and average pore size. The Fourier transform infrared spectroscopy (FTIR) spectra of the as-prepared samples were recorded before and after the adsorption tests on a Shimadzu IRAffinity-1 spectrometer using KBr pellets in the range of 4000–400 cm^{-1} region.

2.4. Adsorption kinetic and equilibrium experiments

Phosphate adsorption kinetic study was carried out by adding a certain amount of adsorbent (100 mg) to a 1000 mL flask filled with 500 mL phosphate solution (10 mg/L). The pH value of the solution was maintained at 7.0 by adding 0.1 M NaOH or 0.1 M HCl solutions. The flask was placed in a thermostatic shaker at 30 °C. A 10 ml of the thoroughly mixed suspensions were sampled with a syringe at certain time intervals and immediately filtered by a 0.45 μm membrane. Phosphate concentrations in the solutions were determined spectrophotometrically by the molybdenum blue method, monitoring the absorbance at 700 nm on UV-vis spectrophotometer [15]. The amount of phosphate adsorbed on samples at time t, q_t (mg/g), was calculated from the following equation:

$$q_t = \frac{(C_0 - C_t)V}{W} \quad (1)$$

where C_0 and C_t (mg/L) are the concentrations of phosphate at initial and given time t, respectively, V is the volume of the solution (L) and W is the mass of adsorbent used (g).

Adsorption isotherm measurements were carried out by adding 20 mg adsorbent to a series of 100 mL flask filled with 50 mL diluted phosphate solutions (10–300 mg/L) at natural pH (ca. 7). The amount of phosphate at equilibrium q_e (mg/g) on the adsorbent samples was calculated from the following equation:

$$q_e = \frac{(C_0 - C_e)V}{W} \quad (2)$$

where C_0 and C_e (mg/L) are the liquid phase concentrations of phosphate at initial and equilibrium, respectively, V is the volume of the solution (L) and W is the mass of adsorbent used (g).

3. Results and discussion

3.1. XRD

The XRD patterns of Zn–Al LDH, Zn–Al LDO and Zn–Al LDO after reconstruction by phosphate solution are illustrated in Fig. 1. It can be seen from Fig. 1a that a series of (0 0 l) peaks appear as sharp and intense symmetric lines at low 2θ values and clear (1 1 0) reflections at high 2θ values, indicating characteristic basal reflections of hydrotalcite-like LDH materials [38]. The reflections were indexed to a hexagonal lattice with rhombohedral 3R symmetry. The interlayer d-spacing of characteristic (0 0 3) planes (d_{003}) at $2\theta = 11.56°$ was found to be 7.60 Å. This typical interplanar spacing was readily

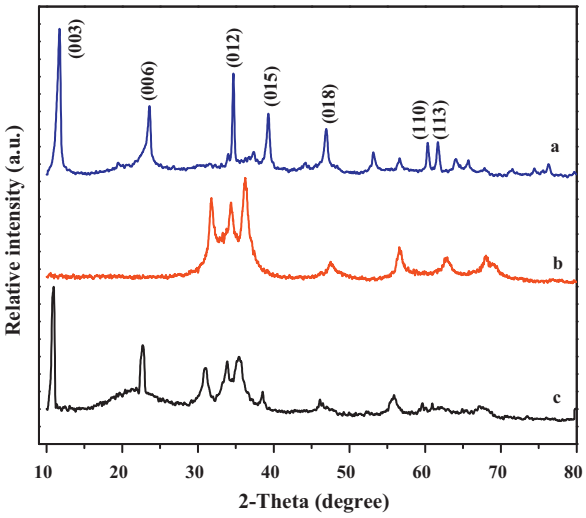

Fig. 1. XRD patterns of (a) sample LDH (0.4), (b) LDO (0.4), and (c) LDO (0.4) after reconstruction by phosphate aqueous solution.

attributed to the sum of the basal lattice parameters of brucite-type main layers (4.80 Å) and the diameter of the intercalated anion (CO_3^{2-}, 2.80 Å) [39]. The XRD pattern in Fig. 1b indicates that the phases of LDHs completely disappeared and were replaced by phases of metal oxides after calcination at 300 °C for 6 h. It is worth noting that the LDO samples present LDH phase structure with broadened reflections of a similar pattern as the original precursor when immersed in phosphate solution (Fig. 1c), implying that the Zn–Al oxide undergo spontaneous rehydration reaction and structural reconstruction arising from so-called "memory effect" [40]. Furthermore, the calculated value of basal spacing of (0 0 3) reflections (7.65 Å) is slightly larger than that of the original Zn–Al LDH, while intensity of the diffraction peaks decreases, indicating the phosphate was partially intercalated into the interlayer of the Zn–Al LDHs and a very small amount of dissolved carbonate anions is still located between the layers.

3.2. SEM

Fig. 2 shows SEM images of samples prepared by different urea concentration. As seen, Zn–Al LDH sample obtained in the pres-

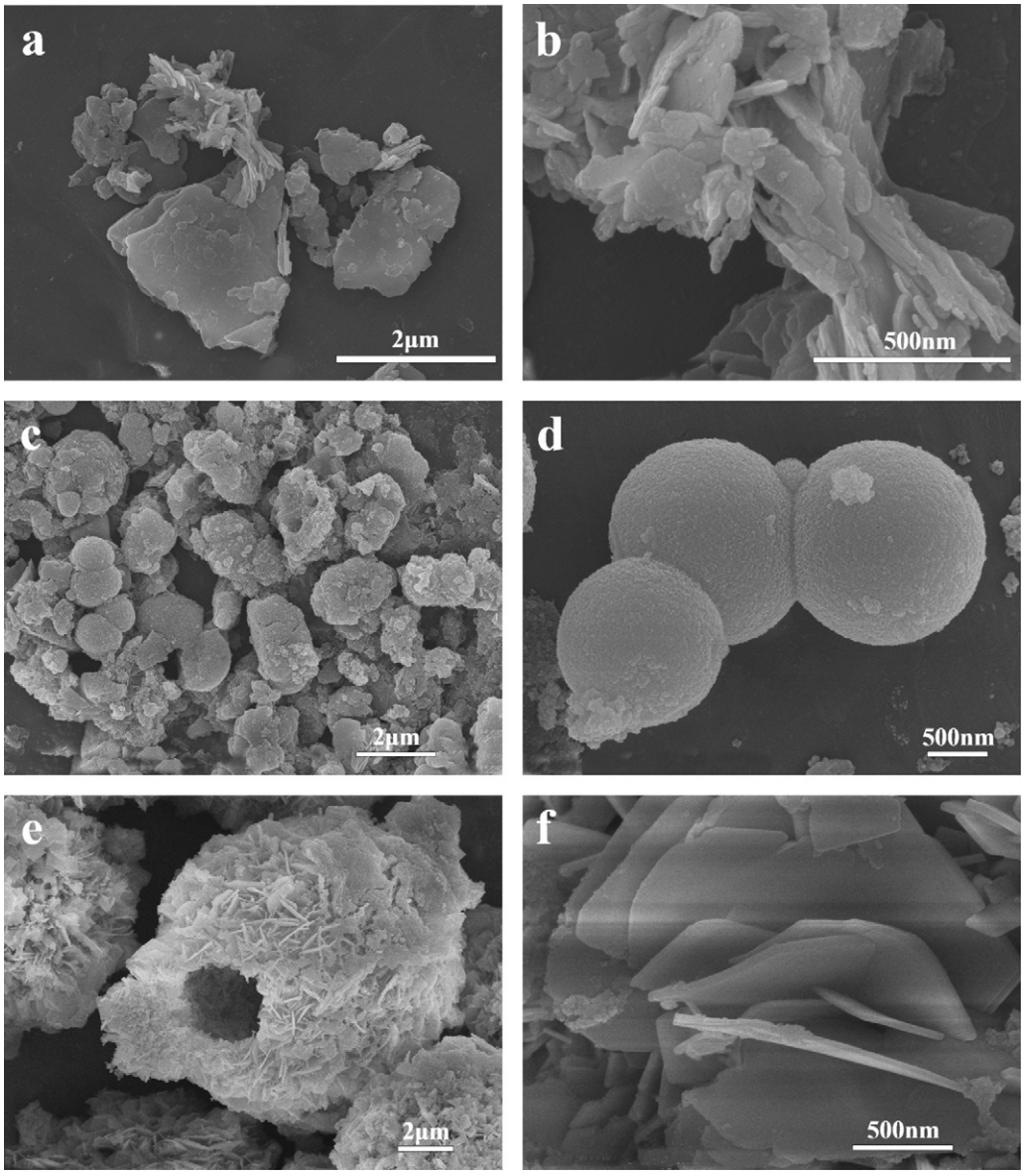

Fig. 2. SEM images of Zn–Al LDH samples prepared with varying urea concentration: (a and b) 0.1 M, (c and d) 0.2 M and (e and f) 0.4 M.

ence of 0.1 M urea exhibited irregular nanosheets with ca. 250 nm in length, 80 nm in width, and 10 nm in thickness (Fig. 2a and b). An increase of urea to 0.2 M led to the formation of solid microspheres with diameter of ca. 1.0–1.5 μm (Fig. 2c and d). Interestingly, when the concentration of urea was further increased to 0.4 M, the morphology was changed to hollow microspheres with diameter of ca. 8 μm and shell thickness of ca. 1.5 μm (Fig. 2e and f). The external surface of these microspheres consists of closely packed and interconnected nanosheets. This study demonstrates that the formation of Zn–Al LDHs with a variety of morphologies from irregular nanosheets, to solid microspheres, to hollow microspheres is highly dependent on the concentration of urea and intrinsic crystal structure of LDH materials.

3.3. Specific surface areas and porosity

The typical nitrogen adsorption–desorption isotherms and their corresponding pore size distributions (PSD) for the samples are shown in Fig. 3. The Zn–Al LDHs and LDOs samples displayed type IV isotherms. A small H2-type hysteresis loops is observed in the range of 0.4–0.9 (Fig. 3a), indicating the presence of ink-bottle pores with narrow necks. Meanwhile, at high relative pressure between 0.9 and 1.0, the shape of hysteresis loops resembles type H3, which is associated with slit-like pores. In addition, the observed hysteresis loop shifted to a higher relative pressure ($P/P_0 > 0.9$) was due to increase in the nitrogen adsorption in macropores (>50 nm) [41]. As seen from Fig. 3b, the PSD curves are quite broad and multimodal with small mesopores (peak pore at ca. 3.5 nm) and larger ones (peak pore at ca. 30 nm). The smaller mesopores reflect pores present within nanosheets, while larger mesopores can be correlated to the pores formed between stacked nanosheets. The macroporous structure (ca. 100–500 nm) can be directly observed on the SEM images of the samples shown in Fig. 2, which cannot be accessed by N_2 adsorption–desorption analysis.

The pore structure parameters of the samples, such as specific surface area, pore volume and average pore size, are listed in Table 1. It is noteworthy that the specific surface areas of all LDOs samples are larger than 130 m^2/g. Generally, for adsorbent, a large surface area can offer more active adsorption sites. Furthermore, the unique three-dimensional frameworks with porosity on multiple length scales are crucial for adsorption applications in wastewater treatment.

3.4. Formation mechanism

On the basis of the above characterization results, the possible formation mechanism of hierarchical Zn–Al LDHs hollow microspheres are illustrated in Fig. 4. In this study, the urea plays an essential role in the morphological transformation by providing a steady OH^- ion source through gradual hydrolyzation. Consequently, the reaction between the zinc, aluminum ions and OH^- ion is steady in aqueous solutions [42]. Zinc and aluminum ions will coprecipitate and form the LDH crystal nucleus, which provide the necessary heterogeneous nucleation sites [43]. The hydrothermal system with weakly basic solution favors the formation of spherical amorphous particles [26]. In particular, an increase in the urea concentration accelerates the Zn–Al LDHs nucleation rates and thus results in the formation of loose nanosheet aggregates in order to

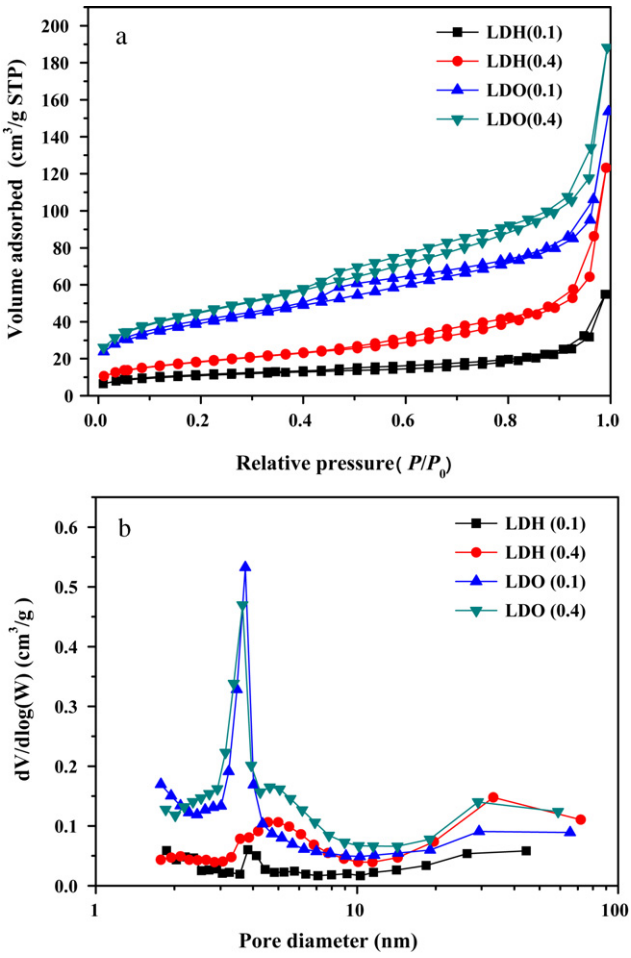

Fig. 3. Nitrogen adsorption and desorption isotherms (a) and pore size distribution curves (b) of the Zn–Al LDHs and LDOs samples.

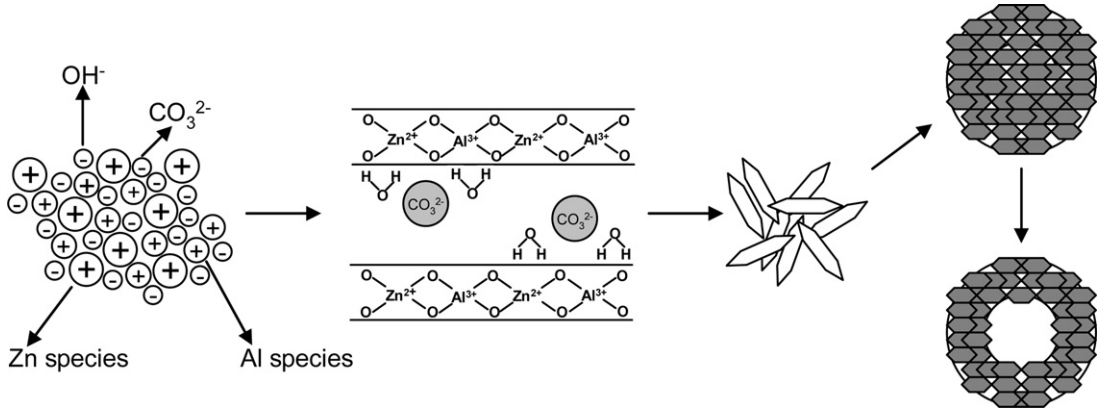

Fig. 4. Schematic illustration of hierarchical Zn–Al layered double hydroxides hollow microspheres.

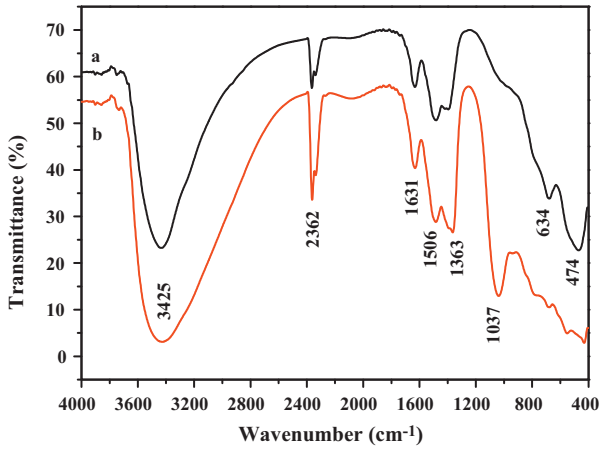

Fig. 5. FTIR spectra of the sample LDO (0.4) before (a) and after (b) adsorption of phosphate.

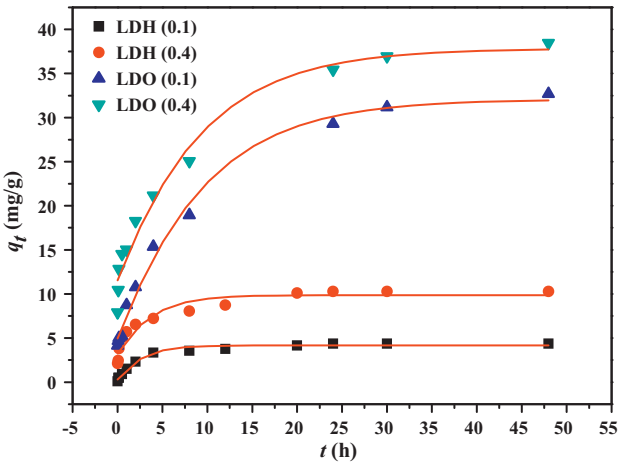

Fig. 6. Effects of contact time on the adsorption of phosphate by Zn–Al LDHs and LDOs samples (C_0 = 10 mg/L, T = 30 °C and pH 7).

minimize their surface energy. Moreover, the nature of LDHs is the direct driving force for the formation of porous arrays with a house-of-cards structure, resulting in abundant inter-particle porosity [44]. Thus, the aggregates continuously grow in size and density to form spheres with dense cores. Since the interior materials have relatively high surface energy and the exterior surface of the particles are protected by the adsorbed Zn^{2+} and Al^{3+} species, it is not surprising that the dissolution will occur preferably in the interior. Therefore, the inside-out Ostwald ripening coupled self-assembly process was proposed to result in the formation of hierarchical LDH microspheres.

3.5. FTIR spectra

The phosphate adsorption process was qualitatively confirmed by FT-IR spectra as shown in Fig. 5. The peak located at 1037 cm^{-1} is attributed to the bending vibration of adsorbed phosphate P–O [45]. Broad and intense absorption bands at 3425 cm^{-1} (O–H stretching vibration) and a band at 1631 cm^{-1} (O–H bending vibration) indicate the presence of interstitial water molecules [46]. Some lattice vibrations of metal–oxygen bonds M–O are also observed at 634 and 474 cm^{-1} [47]. It is noteworthy that the extra bands at ca. 1363 and 2362 cm^{-1} are observed, implying CO_3^{2-} species in the interlayer [48].

3.6. Phosphate adsorption kinetics

The adsorption kinetics is important for adsorption studies because it can predict the rate at which a pollutant is removed from aqueous solutions and provide valuable data for understanding the mechanism of sorption reactions [49]. The adsorption kinetics of phosphate on Zn–Al LDHs and LDOs samples obtained by batch tests for an initial phosphate concentration of 10 mg/L at pH 7 are shown in Fig. 6.

In order to examine the diffusion mechanism involved during the adsorption process, various kinetic models were tested. Firstly, the adsorption data were fitted to pseudo-first-order kinetic model, which is defined as:

$$lg(q_e - q_t) = lg\ \ q_e - \frac{k_1}{2.303}t \tag{3}$$

where q_e and q_t are the amount of phosphate adsorbed (mg/g) at equilibrium and at time t (h), respectively, and k_1 (h^{-1}) is the pseudo-first-order rate constant. Values of k_1 are calculated from the plots of lg $(q_e - q_t)$ versus t (Fig. 7) for the adsorbent samples. The R^2 values obtained are relatively small and the experimental q_e values do not agree with the values calculated from the linear plots.

Secondly, the pseudo-second-order kinetic model is expressed as the following:

$$\frac{t}{q_t} = \frac{1}{k_2 q_e^2} + \frac{t}{q_e} \tag{4}$$

where q_e and q_t are the amount of phosphate adsorbed on adsorbent (mg/g) at equilibrium and at time t (h), respectively, and k_2 is the pseudo-second-order rate constant (g/mg h). Based on the experimental data of q_t and t, the equilibrium adsorption capacity (q_e) and the pseudo-second-order rate constant (k) can be determined from the slope and intercept of a plot of t/q_t versus t. It was found that the pseudo-second-order model gives a satisfactory fit to all of the experimental data. The linear plots of phosphate adsorption kinetics to the pseudo-second-order model and the calculated kinetic parameters are given in Fig. 8 and Table 2, respectively.

Thirdly, intra-particle diffusion model based on the theory proposed by Weber and Morris [50] is applied to elucidate the diffusion mechanism. According to this theory:

$$q_t = k_{di}\sqrt{t} + c_i \tag{5}$$

where k_{di} is intra-particular diffusion rate constant (mg/g $h^{1/2}$). If intra-particle diffusion is rate-limited, then plots of adsorbate uptake q_t versus the square root of time ($t^{1/2}$) would result in a

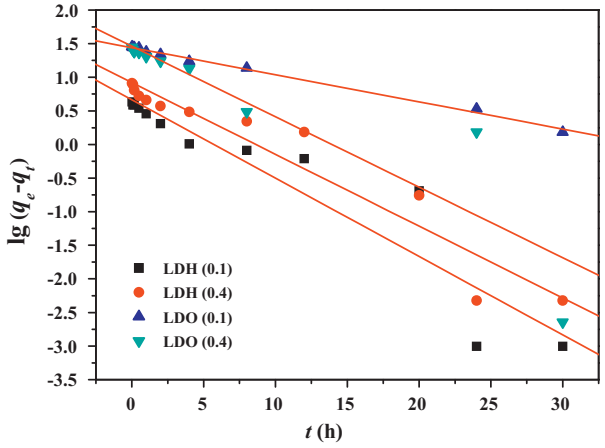

Fig. 7. Pseudo-first-order kinetics for adsorption of phosphate by Zn–Al LDHs and LDOs samples.

Table 2
Pseudo-second-order adsorption kinetic constants of Zn–Al LDHs and LDOs samples.

Samples	C_0 (mg/L)	$q_{e,exp}$ (mg/g)	Pseudo-second-order model			
			$q_{e,cal}$ (mg/g)	k_2 (g/mg h^{-1})	R^2	S.D. (%)
LDH (0.1)	10	4.37	4.52	0.1414	0.9952	0.25
LDH (0.4)		10.28	10.30	0.1113	0.9911	0.41
LDO (0.1)		32.70	33.82	0.0107	0.9862	0.47
LDO (0.4)		38.48	38.96	0.0159	0.9925	0.49

Table 3
Intra-particle diffusion model constants and correlation coefficients for adsorption of phosphate on Zn–Al LDHs and LDOs samples.

Samples	C_0 (mg/L)	Intra-particle diffusion model								
		k_{d1} (mg/h$^{1/2}$ g)	C_1	$(R_1)^2$	k_{d2} (mg/h$^{1/2}$ g)	C_2	$(R_2)^2$	k_{d3} (mg/h$^{1/2}$ g)	C_3	$(R_3)^2$
LDH (0.1)	10	1.72	0	1	1.68	−0.193	0.997	0.39	2.42	1
LDH (0.4)		9.20	0	1	2.15	3.50	0.998	1.05	5.09	1
LDO (0.1)		16.17	0	1	5.38	3.43	0.993	1.04	25.40	1
LDO (0.4)		36.18	0	1	5.07	10.67	0.997	1.05	31.18	1

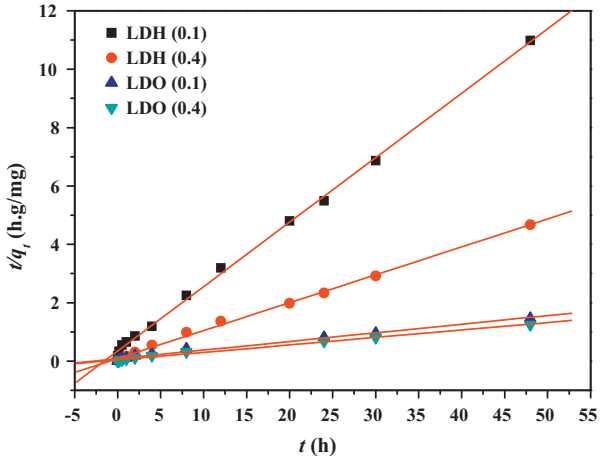

Fig. 8. Pseudo-second-order kinetics for adsorption of phosphate by Zn–Al LDHs and LDOs samples.

linear relationship. Therefore, k_{di} and c_i values can be respectively calculated from the slope and intercept of these plots (Fig. 9) and are listed in Table 3. C_i gives an idea about the thickness of boundary layer. If the value of c is zero, then the rate of adsorption is controlled by intra-particle diffusion for the entire adsorption process. Generally, the plot of q_t against $t^{1/2}$ usually shows more than one linear portion, and if the slope of the first portion is not zero, then film (boundary layer) diffusion controls the adsorption rate at the beginning.

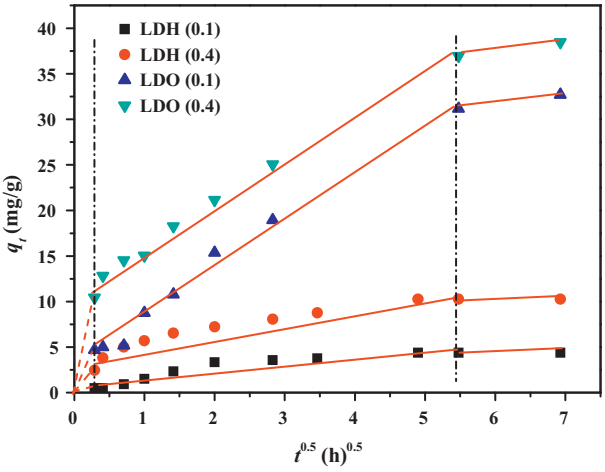

Fig. 9. Intra-particle diffusion plot for adsorption of phosphate onto Zn–Al LDHs and LDOs samples.

Fig. 9 presents a linear fit of intra-particle diffusion model for adsorption of phosphate onto LDHs and LDOs samples. Such types of plots present multilinearity, indicating that two or more steps take place. The first region is the instantaneous adsorption or external surface adsorption stage, which was driven by initial phosphate concentration difference. The second region is the gradual adsorption stage where intraparticle diffusion is the rate limiting step. The third region is the final equilibrium stage where intraparticle diffusion further slows down due to the extremely low adsorbate concentrations left in the solutions [51]. As seen from Fig. 9, the plots are not linear over the whole time range, implying that more than one process affects the adsorption. The rate parameters for phosphate adsorption (Table 3) show that the values of k_{d1} and k_{d2} with LDOs samples are larger than that with LDHs samples. This is because LDOs samples have a larger surface area and pore volume for solute adsorption instantaneously.

Furthermore, normalized standard deviation, S.D. (%), is usually used to evaluate the conformity between experiment data and model fitting values and thereby find the most applicable model to describe the kinetic data of phosphate adsorption on the LDHs and LDOs samples. It is clear from the values of S.D. (%) in Table 2 and R^2 values in Table 3 that phosphate adsorption kinetics on LDHs and LDOs samples were better described by pseudo-second-order equation and intra-particle diffusion model.

3.7. Adsorption isotherm

Adsorption capacity at different aqueous equilibrium concentrations can be illustrated by the adsorption isotherm. The adsorption isotherms of Zn–Al LDHs and LDOs to phosphate are shown in Fig. 10. The adsorption isotherm data were further fitted by two equilibrium models, Langmuir model (6) [52] and Freundlich (7) [53]:

$$\frac{C_e}{q_e} = \frac{C_e}{q_{max}} + \frac{1}{K_L q_{max}} \quad (6)$$

$$lg\ \ q_e = lg\ \ K_F + \frac{1}{n}\ \ lg\ \ C_e \quad (7)$$

where q_e is the amount of phosphorus adsorbed at equilibrium (mg/g), q_{max} the theoretical maximum monolayer sorption capacity (mg/g), C_e the equilibrium concentration of phosphorus in solution

Table 4
Adsorption isotherm parameters of Zn–Al LDHs and LDOs samples.

Samples	Langmuir isotherm model				Freundlich isotherm model		
	K_L (L/mg)	q_{max} (mg/g)	R^2	R_L	n	K_F (mg/g) (L/mg)$^{1/n}$	R^2
LDH (0.1)	0.0242	54.1	0.9978	0.121	2.039	3.567	0.9012
LDH (0.4)	0.0258	76.1	0.9972	0.114	2.011	4.982	0.8957
LDO (0.1)	0.0313	146.8	0.9909	0.096	2.293	13.404	0.9776
LDO (0.4)	0.0292	232.0	0.9923	0.102	1.894	14.226	0.9640

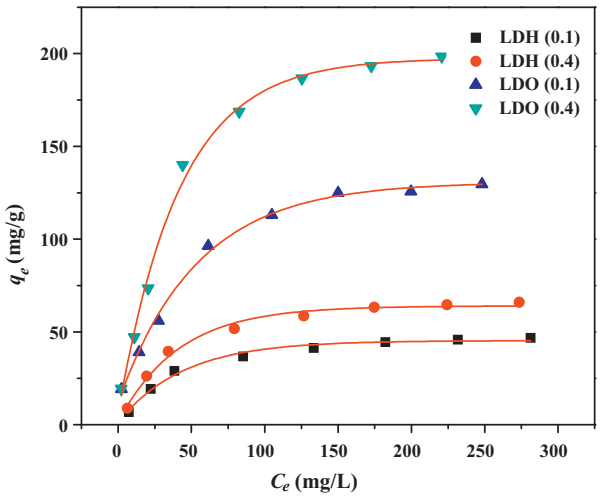

Fig. 10. Adsorption isotherm of phosphate by Zn–Al LDHs and LDOs samples (C_0 = 10–300 mg/L, T = 30 °C and pH 7).

(mg/L). K_L, n and K_F are empirical constants. K_L measures the affinity of the sorbent for the solute.

The adsorption of phosphate by LDHs and LDOs samples increases as the initial phosphate concentration increased as shown in Fig. 10. Table 4 summarizes Langmuir and Freundlich isothermal parameters for the phosphate adsorption on LDHs and LDOs samples. It can be observed that Langmuir equation gives more satisfactory fitting to the adsorption isotherms of phosphate on LDHs and LDOs samples with correlation coefficient R^2 higher than 0.98, indicating the homogeneous nature of sample surface and formation of monolayer coverage of phosphate molecule on the outer surface of adsorbent. Table 4 shows the values of R_L (0.096–0.121), a dimensionless separation factor, are in the range of 0–1, confirming the favorable uptake of the phosphate [54]. Further investigations show that adsorption capacity for LDOs samples are higher than that of LDHs at the same equilibrium concentration of phosphate. Based on the values of q_{max} (Table 4), theoretical phosphate adsorption capacity for LDOs samples are about three times than that of LDHs calculated by the Langmuir equation. The difference is due to the increase of specific surface area by calcinations treatment and simultaneously the release of intercalated anions (mainly CO_3^{2-}) from the precursor interlayer space, which produces more active sites for phosphate adsorption during the LDHs reconstruction process [55]. Interestingly, the theoretic maximum absorption capacity for LDO (0.4) sample has reached to 232 mg/g, which can be attributed to its high surface area micro- and meso-porosity with abundant adsorption sites and macroporous networks with accessible diffusion pathways for adsorbates.

4. Conclusions

A facile hydrothermal method was developed using urea as precipitating agent for the synthesis of hierarchical zinc–aluminum layered double hydroxides with various morphologies from irregular nanosheets to solid microspheres to hollow microspheres. The urea plays a key role in the respective morphological transformation. The as-prepared Zn–Al LDHs and LDOs show excellent adsorption capacity towards phosphate in aqueous solutions. The underlying adsorption kinetics follows the pseudo-second-order kinetic model and intra-particle diffusion model. Furthermore, the experimental equilibrium data are well described by Langmuir isotherm. Owing to their unique hierarchical porous structures, high surface areas and low-cost, LDHs and LDOs are potentially applicable in wastewater treatment.

Acknowledgements

This work was partially supported by the National Natural Science Foundation of China (20877061 and 51072154) and the Natural Science Foundation of Hubei Province (2010CDA078), the National Basic Research Program of China (2007CB613302), and the China Postdoctoral Science Foundation project (20090460998).

References

[1] S.S.S. Lau, S.N. Lane, Biological and chemical factors influencing shallow lake eutrophication: a long-term study, Sci. Total Environ. 288 (2002) 167–181.
[2] V.H. Smith, G.D. Tilman, J.C. Nekola, Eutrophication: impacts of excess nutrient inputs on freshwater, marine, and terrestrial ecosystems, Environ. Pollut. 100 (1999) 179–196.
[3] Y.N. Zhou, X.H. Xing, Z.H. Liu, L.W. Cui, A.F. Yu, Q. Feng, H.J. Yang, Enhanced coagulation of ferric chloride aided by tannic acid for phosphorus removal from wastewater, Chemosphere 72 (2008) 290–298.
[4] N. Boujelben, J. Bouzid, Z. Elouear, M. Feki, F. Jamoussi, A. Montiel, Phosphorus removal from aqueous solution using iron coated natural and engineered sorbents, J. Hazard. Mater. 151 (2008) 103–110.
[5] G.G. Timby, T.C. Daniel, R.W. McNew, P.A. Moore Jr., Polymer type and aluminum chloride affect screened solids and phosphorus removal from liquid dairy manure, Appl. Eng. Agric. 20 (2004) 57–64.
[6] G.M. Ayoub, B. Koopman, N. Pandya, Iron and aluminum hydroxy (oxide) coated filter media for low-concentration phosphorus removal, Water Environ. Res. 73 (2001) 478–485.
[7] G.Z. Gong, S.F. Ye, Y.J. Tian, Q. Wang, J.D. Ni, Y.F. Chen, Preparation of a new sorbent with hydrated lime and blast furnace slag for phosphorus removal from aqueous solution, J. Hazard. Mater. 166 (2009) 714–719.
[8] D. Seyhan, A. Erdincler, Effect of lime stabilisation of enhanced biological phosphorus removal sludges on the phosphorus availability to plants, Water Sci. Technol. 48 (2003) 155–162.
[9] E. Yildiz, Phosphate removal from water by fly ash using crossflow microfiltration, Sep. Purif. Technol. 35 (2004) 241–252.
[10] W.W. Huang, S.B. Wang, Z.H. Zhu, L. Li, X.D. Yao, V. Rudolph, F. Haghseresht, Phosphate removal from wastewater using red mud, J. Hazard. Mater. 158 (2008) 35–42.
[11] A. Ugurlu, B. Salman, Phosphorus removal by fly ash, Environ. Int. 24 (1998) 911–918.
[12] Y.J. Xue, H.B. Hou, S.J. Zhu, Characteristics and mechanisms of phosphate adsorption onto basic oxygen furnace slag, J. Hazard. Mater. 162 (2009) 973–980.
[13] A. Drizo, C. Forget, R.P. Chapuis, Y. Comeau, Phosphorus removal by electric arc furnace steel slag and serpentinite, Water Res. 40 (2006) 1547–1554.
[14] B. Kostura, H. Kulveitova, J. Lesko, Blast furnace slags as sorbents of phosphate from water solutions, Water Res. 39 (2005) 1795–1802.
[15] Y. Yang, Y.Q. Zhao, P. Kearney, Influence of ageing on the structure and phosphate adsorption capacity of dewatered alum sludge, Chem. Eng. J. 145 (2008) 276–284.
[16] E.E. Codling, R.L. Chaney, C.L. Mulchi, Use of aluminum- and iron-rich residues to immobilize phosphorus in poultry litter and litter-amended soils, J. Environ. Qual. 29 (2000) 1924–1931.
[17] N.Y. Mezenner, A. Bensmaili, Kinetics and thermodynamic study of phosphate adsorption on iron hydroxide–eggshell waste, Chem. Eng. J. 147 (2009) 87–96.

[18] K. Karageorgiou, M. Paschalis, G.N. Anastassakis, Removal of phosphate species from solution by adsorption onto calcite used as natural adsorbent, J. Hazard. Mater. 139 (2007) 447–452.
[19] R.C. Wu, J.H. Qu, Y.S. Chen, Magnetic powder MnO–Fe_2O_3 composite-a novel material for the removal of azo-dye from water, Water Res. 39 (2005) 630–638.
[20] J.B. Joo, J. Park, J. Yi, Preparation of polyelectrolyte-functionalized mesoporous silicas for the selective adsorption of anionic dye in an aqueous solution, J. Hazard. Mater. 168 (2009) 102–107.
[21] J.G. Yu, Y.R. Su, B. Cheng, Template-free fabrication and enhanced photocatalytic activity of hierarchical macro-/mesoporous titania, Adv. Funct. Mater. 17 (2007) 1984–1990.
[22] J.G. Yu, L.J. Zhang, B. Cheng, Y.R. Su, Hydrothermal preparation and photocatalytic activity of hierarchically sponge-like macro-/mesoporous titania, J. Phys. Chem. C 111 (2007) 10582–10589.
[23] W.Q. Cai, J.G. Yu, S. Mann, Template-free hydrothermal fabrication of hierarchically organized-AlOOH hollow microspheres, Micropor. Mesopor. Mater. 122 (2009) 42–47.
[24] W.Q. Cai, J.G. Yu, B. Cheng, B.L. Su, M. Jaroniec, Synthesis of boehmite hollow core/shell and hollow microspheres via sodium tartrate-mediated phase transformation and their enhanced adsorption performance in water treatment, J. Phys. Chem. C (113) (2009) 14739–14746.
[25] W.Q. Cai, J.G. Yu, M. Jaroniec, Template-free synthesis of hierarchical spindle-like γ–Al_2O_3 materials and their adsorption affinity towards organic and inorganic pollutants in water, J. Mater. Chem. 20 (2010) 4587–4594.
[26] W.Q. Cai, J.G. Yu, S.H. Gu, M. Jaroniec, Facile hydrothermal synthesis of hierarchical boehmite: sulfate-mediated transformation from nanoflakes to hollow microspheres, Cryst. Growth Des. 10 (2010) 3977–3982.
[27] J.G. Yu, W. Liu, H.G. Yu, A one-pot approach to hierarchically nanoporous titania hollow microspheres with high photocatalytic activity, Cryst. Growth Des. (8) (2008) 930–934.
[28] S.W. Liu, J.G. Yu, S. Mann, Spontaneous construction of photoactive hollow TiO_2 microspheres and chains, Nanotechnology 20 (2009) 325606.
[29] J.G. Yu, L.F. Qi, Template-free fabrication of hierarchically flower-like tungsten trioxide assemblies with enhanced visible-light-driven photocatalytic activity, J. Hazard. Mater. 169 (2009) 221–227.
[30] J.G. Yu, H.G. Yu, H.T. Guo, M. Li, S. Mann, Spontaneous formation of a tungsten trioxide sphere-in-shell superstructure by chemically induced self-transformation, Small (4) (2008) 87–91.
[31] B. Cheng, Y. Le, W.Q. Cai, J.G. Yu, Synthesis of hierarchical $Ni(OH)_2$ and NiO nanosheets and their adsorption kinetics and isotherms to Congo red in water, J. Hazard. Mater. 185 (2011) 889–897.
[32] J.B. Zhou, S.L. Yang, J.G. Yu, Facile fabrication of mesoporous MgO microspheres and their enhanced adsorption performance for phosphate from aqueous solutions, Colloids Surf. A: Physicochem. Eng. Aspects 379 (2011) 102–108.
[33] J. Das, B.S. Patra, N. Baliarsingh, K.M. Parida, Adsorption of phosphate by layered double hydroxides in aqueous solutions, Appl. Clay Sci. 32 (2006) 252–260.
[34] R. Chitrakar, S. Tezuka, A. Sonoda, K. Sakane, K. Ooi, T. Hirotsu, Synthesis and phosphate uptake behavior of Zr^{4+} incorporated MgAl-layered double hydroxides, J. Colloid Interface Sci. 313 (2007) 53–63.
[35] P. Koilraj, S. Kannan, Phosphate uptake behavior of ZnAlZr ternary layered double hydroxides through surface precipitation, J. Colloid Interface Sci. 341 (2010) 289–297.
[36] Y. Seida, Y. Nakano, Removal of phosphate by layered double hydroxides containing iron, Water Res. 36 (2002) 1306–1312.
[37] R. Chitrakar, S. Tezuka, A. Sonoda, K. Sakane, K. Ooi, T. Hirotsu, Adsorption of phosphate from seawater on calcined MgMn-layered double hydroxides, J. Colloid Interface Sci. 290 (2005) 45–51.
[38] Y.C. Wang, F.Z. Zhang, S.L. Xu, X.Y. Wang, D.G. Evans, X. Duan, Preparation of layered double hydroxide microspheres by spray drying, Ind. Eng. Chem. Res. 47 (2008) 5746–5750.
[39] J.L. Guimaraes, R. Marangoni, L.P. Ramos, F. Wypych, Covalent grafting of ethylene glycol into the Zn–Al–CO_3 layered double hydroxide, J. Colloid Interface Sci. 227 (2000) 445–451.
[40] O.P. Ferreira, O.L. Alves, D.X. Gouveia, A.G. Souza, J.A.C. de Paiva, J. Mendes, Thermal decomposition and structural reconstruction effect on Mg–Fe-based hydrotalcite compounds, J. Solid State Chem. 177 (2004) 3058–3069.
[41] G. Leofanti, M. Padovan, G. Tozzola, B. Venturelli, Surface area and pore texture of catalysts, Catal. Today 41 (1998) 207–219.
[42] C.Y. Cao, Z.M. Cui, C.Q. Chen, W.G. Song, W. Cai, Ceria hollow nanospheres produced by a template-free microwave-assisted hydrothermal method for heavy metal ion removal and catalysis, J. Phys. Chem. C 114 (2010) 9865–9870.
[43] H. Wang, G.L. Fan, C. Zheng, X. Xiang, F. Li, Facile sodium alginate assisted assembly of Ni–Al layered double hydroxide nanostructures, Ind. Eng. Chem. Res. 49 (2010) 2759–2767.
[44] J.P. Liu, X.T. Huang, Y.Y. Li, K.M. Sulieman, X. He, F.L. Sun, Facile and large-scale production of ZnO/Zn–Al layered double hydroxide hierarchical heterostructures, J. Phys. Chem. B 110 (2006) 21865–21872.
[45] H.L. Liu, X.F. Sun, C.Q. Yin, C. Hu, Removal of phosphate by mesoporous ZrO_2, J. Hazard. Mater. 151 (2008) 616–622.
[46] L.A. Rodrigues, M.L.C.P. da Silva, An investigation of phosphate adsorption from aqueous solution onto hydrous niobium oxide prepared by co-precipitation method, Colloids Surf. A: Physicochem. Eng. Aspects 334 (2009) 191–196.
[47] F.M. Labajos, V. Rives, M.A. Ulibarri, Effect of hydrothermal and thermal treatments on the physicochemical properties of Mg–Al hydrotalcite-like materials, J. Mater. Sci. 27 (1992) 1546–1552.
[48] Z. Chang, D.G. Evans, X. Duan, C. Vial, J. Ghanbaja, V. Prevot, M. De Roy, C. Forano, Synthesis of [Zn–Al–CO_3] layered double hydroxides by a coprecipitation method under steady-state conditions, J. Solid State Chem. 178 (2005) 2766–2777.
[49] K.Q. Li, Y. Li, Z. Zheng, Kinetics and mechanism studies of p-nitroaniline adsorption on activated carbon fibers prepared from cotton stalk by $NH_4H_2PO_4$ activation and subsequent gasification with steam, J. Hazard. Mater. 178 (2010) 553–559.
[50] W.J. Weber, J.C. Morris, Proceedings of the International Conference on Water Pollution Symposium, vol. 2, Pergamon, Oxford, 1962, pp. 231–266.
[51] I.A.W. Tan, A.L. Ahmad, B.H. Hameed, Adsorption isotherms, kinetics, thermodynamics and desorption studies of 2, 4, 6-trichlorophenol on oil palm empty fruit bunch-based activated carbon, J. Hazard. Mater. 164 (2009) 473–482.
[52] I. Langmuir, The constitution and fundamental properties of solids and liquids. Part I. Solids, J. Am. Chem. Soc. 38 (1916) 2221–2295.
[53] H.M.F. Freundlich, Uber dye adsorption in losungen, J. Phys. Chem. 57 (1906) 385–470.
[54] M. Islam, R. Patel, Synthesis and physicochemical characterization of Zn/Al chloride layered double hydroxide and evaluation of its nitrate removal efficiency, Desalination 256 (2010) 120–128.
[55] X. Cheng, X.R. Huang, X.Z. Wang, B.Q. Zhao, A.Y. Chen, D.Z. Sun, Phosphate adsorption from sewage sludge filtrate using zinc–aluminum layered double hydroxides, J. Hazard. Mater. 169 (2009) 958–964.